Experimental Characterization and Feasibility Study on High Mechanical Strength Electrical Steels for High-speed Motors Application

Jing Ou, Yingzhen Liu, Patrick Breining, Thomas Gietzelt, Torsten Wunsch, and Martin Doppelbauer

***Abstract*—Sleeves are frequently used for protecting high-speed rotors from high centrifugal forces at high speeds. Currently, metal sleeves such as titanium and inconel alloys and fiber sleeves such as carbon fiber and glass fiber are commonly used. Metal sleeves have high eddy current losses due to armature reaction. Fiber sleeves can avoid high eddy current losses. However, heat dissipation abilities of the rotors are decreased. Moreover, fiber sleeves are sensitive to temperature and manufacturing processes. Hence, sleeve-free interior permanent-magnet (IPM) rotor structure is attractive. To avoid sleeves, electrical steels of high mechanical strength and low core losses are required. Amorphous metal has been proved as a good candidate for such application. It can help to improve the power density and efficiency based on a study of a 15.7 kW, 125,000 rpm IPM demonstrator motor. However, because the mechanical strength of amorphous metal is easily degraded during core manufacturing, a high-silicon steel, 10JNEX900, is considered as an alternative. The electromagnetic and mechanical properties of 10JNEX900 are tested. A prototype made from amorphous metal 2605SA1 is tested to verify the simulation methods and it is used as a benchmark motor to study the feasibility of the new rotor core material.**

***Index Terms*—Amorphous metal, high-silicon steel, high-speed motors, iron losses, mechanical strength.**

I. Introduction

HIGH-SPEED permanent-magnet (PM) motors have been applied for varieties of applications, such as electric engines for aircraft, flywheel energy storage systems, high-speed spindles, turbo-molecular pumps, gas compressors, air blowers, turbochargers and micro-turbines, etc. [1]-[6]. In order to protect high-speed PM rotors from centrifugal forces, sleeves are commonly used. Generally, the commonly used sleeves can be categorized into two types: metal sleeves such as titanium [7]-[10] or inconel alloy [11]-[13], and fiber sleeves such as carbon fiber [14]-[15] or glass fiber [16]. Both types of sleeves have a high yield strength. However, the fiber sleeves are thermally sensitive and their maximum operation temperature is much lower than that of metal sleeves. Moreover, during assembly of the rotors with fiber sleeves, the mechanical strength of the sleeves is easily degraded. Generally, the inner diameters of the sleeves are smaller than the outer diameters of the PMs to provide with a pre-stress. Then the sleeves are pressed axially into the rotors. Alternatively, shrink fitting methods are also feasible to assemble the rotors. Regarding fiber sleeves, the weakest areas locate at the edges of PM segments. PMs may cut into the fiber and cause sleeve failures. A failure of using fiber sleeve is reported in [17]. Hence, metal sleeves are superior to fiber sleeves and they are more frequently used.

A key problem of conductive metal sleeves is their high eddy current losses induced by the nonsynchronous air-gap magnetic fields generated by slotting and current harmonics [18]-[19]. Based on [19] the eddy current losses first increase and then decrease when the conductivity of the sleeves increases. When the permeability of sleeves increases, the flux provided by PMs increases. However, the pole-to-pole flux leakage also increases. Based on [19] non-magnetic sleeves could help to reach the maximum flux provided by PMs. However, the existence of non-magnetic sleeves increases the equivalent air-gap length and reduces the magnetic loading [20]-[21]. It also leads to poor flux weakening ability of the motor. Hence, a sleeve-free high-speed interior permanent-magnet (IPM) rotor is in demand. In [22] an IPM rotor made from amorphous metal 2605SA1 is proposed. By utilizing high mechanical strength and low core losses of the amorphous metal, high power density and high efficiency of the designed demonstrator motor are observed. However, because the mechanical strength of the 2605SA1 cores is easily degraded during prototyping, the tested maximum speed of the prototype is only 115,000 rpm, which is a little lower than the target maximum speed of 125,000 rpm (corresponding to 2083 Hz of the working frequency as the pole-pair number of the rotor PM is 1). Considering massive production of the proposed IPM rotors, an alternative steel with stable and high mechanical strength and low core losses is beneficial. Hence, a high-silicon steel (6.5 % Si), 10JNEX900 is proposed and studied in this paper. In [23] the

This work was supported by German Research Foundation (DFG) under Grant DO 1966/2-1 and the National Natural Science Foundation of China under Grant 51761135112. (*Corresponding author: Yingzhen.Liu*).

Jing Ou, Patrick Breining and Martin Doppelbauer are with the Institute of Electrical Engineering (ETI), Karlsruhe Institute of Technology, Karlsruhe 76131, Germany, (e-mail: jing.ou@kit.edu; patrick.breining@kit.edu; martin.doppelbauer@kit.edu).

Yingzhen Liu is with the Institute of Technical Physics, Karlsruhe Institute of Technology, Karlsruhe 76344, Germany, (e-mail: yingzhen.liu@kit.edu).

Thomas Gietzelt and Torsten Wunsch are with the Institute for Micro Process Engineering, Karlsruhe Institute of Technology, Karlsruhe 76344, Germany, (e-mail: thomas.gietzelt@kit.edu, torsten.wunsch@kit.edu)

high-silicon steel 10JNEX900 is introduced and targeted for high frequency application. By increasing the Si content in the steel sheets, the electrical resistance of the sheets is increased. As a result, the eddy current loss can be reduced. The yield strength of this steel is much higher than that of the conventional steels [1], which makes it suitable for the proposed IPM rotor [24]. In this paper, the feasibility of using 10JNEX900 in high-speed IPM motor is studied. The designed demonstrator motor in [22] is used as a benchmark and the experimental data from the demonstrator is used to validate the simulation methods, which is employed to study the high-speed IPM motor with 10JNEX900.

The paper is organized as follows. The mechanical strength, magnetization ability and core losses of the amorphous metal 2605SA1 and high-silicon steel 10JNEX900 are tested in Section II. Based on the tested data, the performances of the designed demonstrator motor made from the above mentioned two rotor core materials are evaluated and compared in terms of electromagnetic, mechanical and thermal behaviors in Section III. Section IV tests a prototype to verify the accuracy of the analysis results. Finally, the conclusion is drawn in Section V.

II. Electromagnetic and Mechanical Properties of Electrical Steels

A. Selection of electrical steels for high-speed IPM rotor

The selection of electrical steels is very important for the design of electrical machines and there are generally many considerations, such as saturation flux density, core losses, yield strength and price, etc. The advantages and disadvantages of a steel are depending on specific application. In this paper, the yield strength and the core losses are the main consideration. High yield strength of rotor cores is desired to reduce the thickness of the flux bridge so as to avoid a high flux leakage. Meanwhile, for high-speed and high-frequency operation, it is also necessary to consider the high-frequency rotor core losses in order to avoid irreversible PM demagnetization due to high temperature. Amorphous magnetic metal (AMM) 2605SA1, high silicon steels and Nippon steels are potential candidates for high-speed IPM rotors due to their high mechanical strengths as can be seen in Fig. 1. However, Nippon steels are not considered in this paper due to their high core losses.

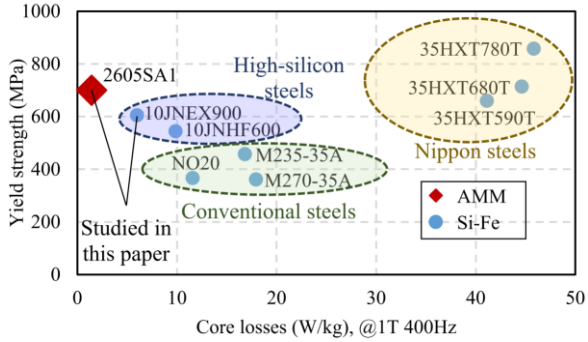

Fig. 1. Yield strength and core losses of high-performance silicon steels [1].

In Fig. 1, there are two high-silicon steels. The difference is summarized in [23]. Because 10JNEX900 has better performance than 10JNHF600 in both yield strength and core losses, 10JNEX900 is considered in this paper. Based on the data provided by the manufacturer, AMM 2605SA1 has not only the lowest core losses, but also higher mechanical strength than high-silicon steels. The feasibility of using 2605SA1 to high-speed IPM rotor has been assessed in [22]. The results show that 2605SA1 is able to improve the power density and efficiency of high-speed IPM motors. A drawback of 2605SA1 for high-speed IPM rotor application is that its mechanical strength is very sensitive to machining and might be significantly reduced during production. 10JNEX900 has stable mechanical strength, which is beneficial for massive production. In this paper 10JNEX900 is considered as an alternative for the proposed rotor core.

The magnetization curves of 10JNEX900 and 2605SA1 provided by the manufacturers are compared in Fig. 2. It can be found that when the magnetic field strength increases, the magnetic flux density of 2605SA1 increases more quickly than that of 10JNE900. However, the saturation flux density of the former is lower than that of the latter.

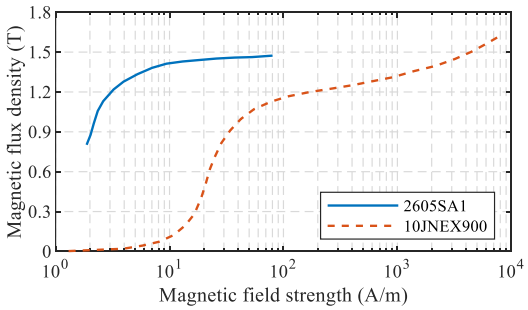

Fig. 2. *B-H* curves of 2605SA1 and 10JNEX900 provided by manufacturers [25], [26].

The overall properties of the two materials are summarized and compared in Table I. Degradation due to prototyping of the materials is not considered in this table. In ideal case, 2605SA1 has higher yield strength, lower core losses, and higher electrical resistivity. 2605SA1 is a better choice for the proposed IPM rotor. However, its thermal conductivity and saturation induction are lower than those of 10JNEX900. Furthermore, 10JNEX900 has a lower Vickers hardness. The cutting of 10JNEX900 is easier. Considering massive production and degradation problem, 10JNEX900 may be a better candidate.

TABLE I
Properties Comparison of 2605SA1 with 10JNEX900 [22], [27], [28]

Material	2605SA1	10JNEX900
Mass density (kg/m^3)	7180	7490
Young's modulus (GPa)	100-110	200-210
Poisson's ratio	0.3	0.33
Yield strength (MPa)	>700	570
Thermal conductivity (W/m·k)	10	18.6
Saturation induction (T)	1.56	1.8
Electrical resistivity (‖, μΩcm)	137	82
Loss $W_{10/400}$ (W)	1.5	5.7
Thickness (mm)	0.023	0.1
Vickers hardness	900	200~300
Max. operating temperature (°C)	150	150

B. *Electromagnetic properties measurement*

To assess the feasibility of using 10JNEX900 and to find out the problems 2605SA1 facing with in the proposed IPM rotor structure, the properties of the two materials are tested and compared. Toroidal cores are used in the test and the dimensions of the cores are based on the standard IEC-60404-6. The dimensions and a picture of the sample core are presented in Fig. 3. The structure of the measurement system is shown in Fig. 4. The toroidal core is wound with two sets of windings. The primary winding is excited with AC current i_1 fed by a linear power amplifier. Sinusoidal voltage u_2 in the secondary winding will be induced by regulating the primary voltage u_1. The regulating variable of the primary voltage u_1 is obtained by comparing the secondary voltage u_2 with a sinusoidal reference. Due to flux leakage, the core magnetization and resistance loss, the primary current i_1 and voltage u_1 may not be sinusoidal. Assuming that the magnetic field in the toroidal core is homogeneous, the *B-H* curve and the core losses can be calculated by using i_1, u_2, and the parameters of the toroidal core. More details about the measurement system can be found in [29].

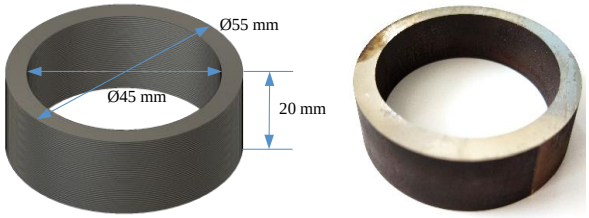

Fig. 3. Dimensions and picture of the toroidal core for electromagnetic properties measurement.

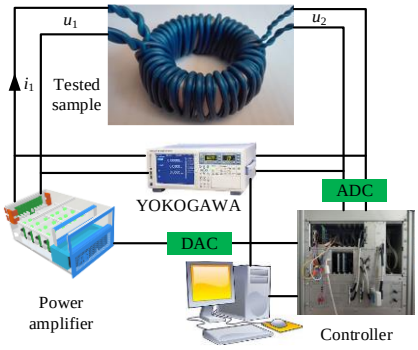

Fig. 4. Structure of the measurement system for electromagnetic properties.

The electromagnetic properties of the two materials of frequencies from 50 Hz to 3 kHz are measured. In Fig. 5 the *B-H* loops at 1 kHz and at room temperature (about 25 ℃) are compared as an example. It can be found that 2605SA1 has much narrower *B-H* loops than 10JNEX900, which means the former has much lower core losses than the latter.

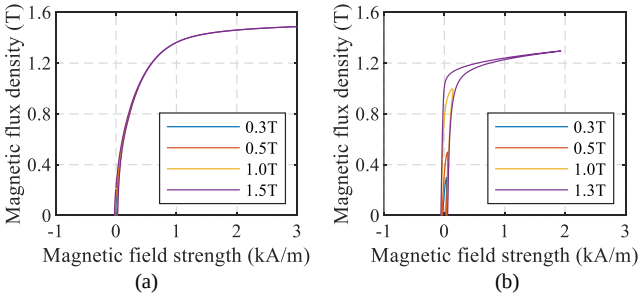

Fig. 5. Measured *B-H* loops at 1 kHz and at 25 ℃. (a) 2605SA1. (b). 10JNEX900.

Because of very small thickness and relatively high resistivity of 2605SA1 and 10JNEX900, their eddy current losses are very low and their commutation curves are almost frequency-independent as illustrated in Fig. 6. To make a clear comparison, two conventional silicon steels of different thicknesses, M330-35A and M330-50A are also tested and the results are compared in Fig. 6. As high thickness leads to high eddy current loss, the commutation curves of M330-35A and M330-50A are frequency-dependent. When the magnetic field strength is fixed, the magnetic flux density at a higher frequency is lower. Because M330-50A is thicker than M330-35A, the eddy current loss of the former are higher than that of the latter as shown in Fig. 6.

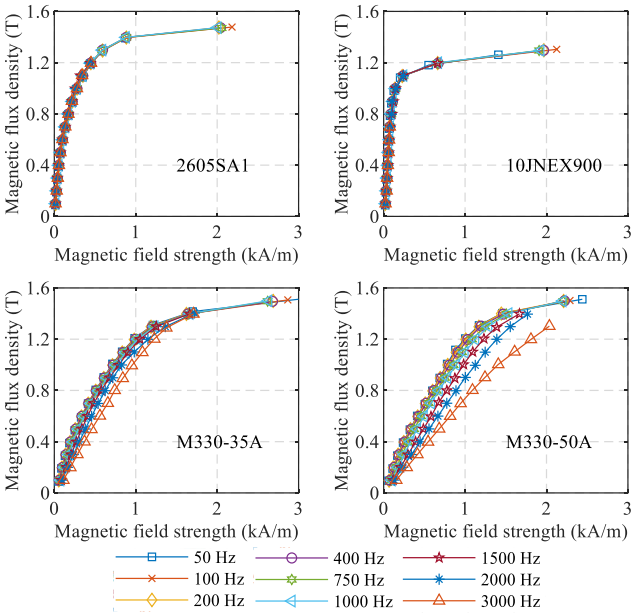

Fig. 6. Measured commutation curves of four materials at 25 ℃ and different frequencies.

C. *Properties degradation*

Based on the data provided by manufacturers and obtained from the above tests, 2605SA1 has lower core losses, lower saturation flux density and higher yield strength in ideal case than 10JNEX900. Regarding high-speed IPM rotor application, the 2605SA1 might be a better choice as it is helpful to reduce the rotor core losses, flux bridge thickness and flux leakage. However, the electromagnetic and mechanical performances of the 2605SA1 are very unstable and they are very easily influenced by mechanical cutting, temperature and stress. The core losses of 2605SA1 are very sensitive to stacking stress. The higher the stacking factor, the higher the stacking stress. Fig. 7 shows the core losses of three 2605SA1 cores with different stacking factors (SFs). They are compared with the raw ribbon to illustrate the degradation problem. It can be found that the higher the stacking factor, the higher the core losses. The core losses of the 2605SA1 core with SF = 0.934 are about 4.6 times the losses of the raw ribbon. Because the 2605SA1 core is degraded when the stacking factor is high, it might even have higher core losses than the 10JNEX900 core after prototyping.

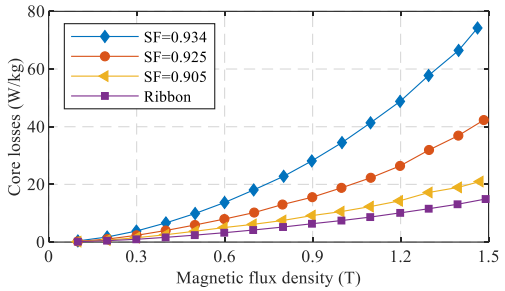

Fig. 7. Measured core losses of the 2605SA1 cores of different stacking factors (SFs) and raw ribbon at 1 kHz and at 25 ℃.

The influences of temperature on the magnetic properties of the two materials are presented in Fig. 8 and Fig. 9. Both materials are temperature sensitive. For example, the *B-H* curves and core losses at 1 kHz and different temperatures of the 2605SA1 core with SF = 0.934 are shown in Fig. 8. It can be noticed that when the temperature is increased, the saturation flux density of 2605SA1 is significantly decreased and the core losses are slightly reduced, whereas the maximum relative permeability is increased. When the working temperature is increased from room temperature (RT, about 25 ℃) to 150 ℃, the saturation flux density is reduced by about 9 % and the core losses are reduced by about 13.3 %.

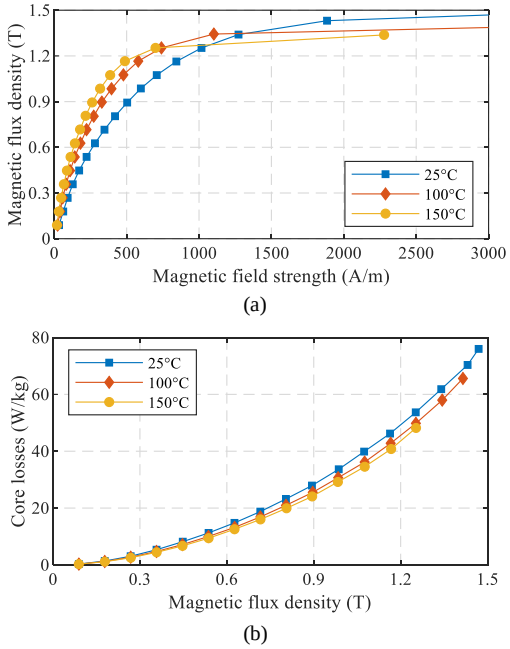

Fig. 8. Measured influences of the temperature on the magnetic properties of 2605SA1 core at 1 kHz. (a) *B-H* curves. (b) Core losses.

The influence of temperature on the magnetic properties of 10JNEX900 core is presented in Fig. 9. It can be seen that the saturation flux density changes slightly while the relative permeability decreases significantly when the temperature is increased. At a higher temperature, a higher magnetic field strength is required to reach a specific flux density. Much different from 2605SA1 core, the core losses of 10JNEX900 are increased when the temperature is increased. When the temperature is increased from RT to 150°C, the core losses are increased by 24.7 % and the relative permeability is reduced by about 60 %.

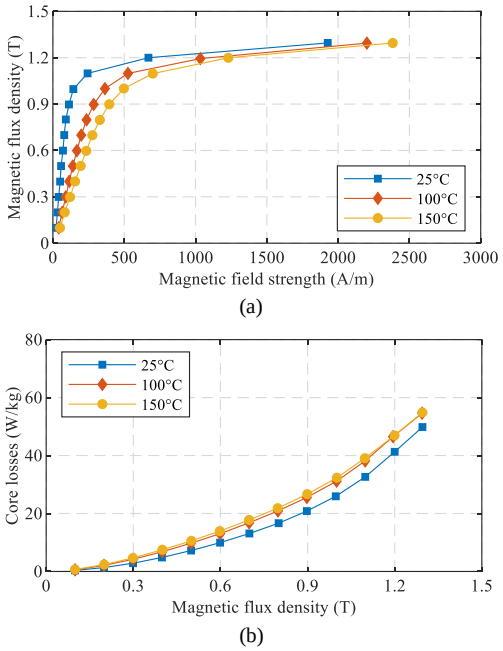

Fig. 9. Measured influences of the temperature on the magnetic properties of 10JNEX900 core at 1 kHz. (a) *B-H* curves. (b) Core losses.

D. Mechanical properties measurement

Because the amorphous metal 2605SA1 is highly brittle, its mechanical strength might be significantly reduced during rotor core cutting and rotor assembly. In [30] single-layer and 3-layer 2605SA1 samples without obvious defect are tested. The tested ultimate mechanical strength (UTS) of single-layer 2605SA1 sample can be higher than 1000 MPa as illustrated in Fig. 10. The tested mechanical strength of 3-layer samples is lower than that of single-layer sample. However, the tested results are still comparable to the value of 700 MPa provided by the manufacturer. To assess the feasibility of using 2605SA1 for high-speed IPM rotor, a demonstrator motor, whose maximum targeted speed is 125,000 rpm, is designed in [18]. A prototype is built and tested. The maximum speed reaches 115,000 rpm, which is a little lower than the targeted speed. To find out the failure reason, a multi-layer sample is separated layer by layer. Transverse cracks around the cutting contour of some layers are found as can be seen in Fig. 11. The transverse cracks significantly reduce the mechanical strength of the cores as 2605SA1 is highly brittle. When 20-layer samples are tested, because defected layers exist in the core, the tested results are much lower than 700 MPa as presented in Fig. 12.

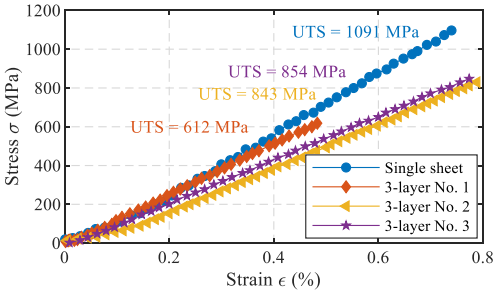

Fig. 10. Tested mechanical strength of 2605SA1 without obvious defects [24].

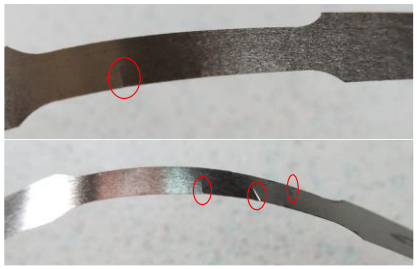

Fig. 11. Transverse cracks of 2605SA1 ribbon.

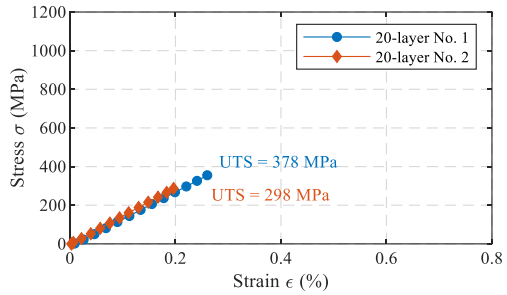

Fig. 12. Tested mechanical strength of 2605SA1 samples with 20 layers.

Based on the tested results of 20-layer samples, it is believed that the failure of the prototype is mainly caused by reduced mechanical strength due to the influence of cutting. To solve this problem, three efforts can be made. The first choice is to remove the defected layers. But this method is unsuitable for massive production. Secondly, by adjusting the cutting parameters to improve the cutting quality so as to reduce the number of total defected layers. In this case, the mechanical strength will not be significantly reduced. However, because of lacking relevant machines, the authors need assistance from a third company. Hence, a third method is considered in this paper that another rotor core material, 10JNEX900, will be used to replace the 2605SA1 rotor core and the feasibility is studied. The tested results of two 10JNEX900 samples are presented in Fig. 13. Their stress-strain curves are quite similar. This means the mechanical strength of 10JNEX900 is very stable. The tested yield strength of them is 570 MPa. Moreover, the stress-strain curves of 10JNEX900 are much different from those of 2605SA1. 10JNEX900 fails at plastic region, whereas 2605SA1 fails at elastic region.

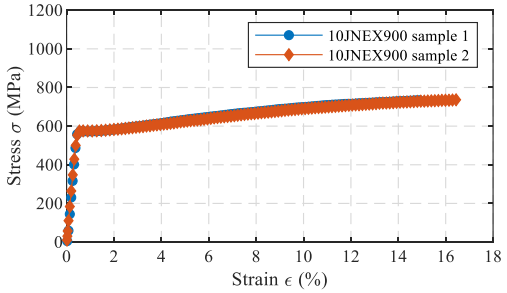

Fig. 13. Tested mechanical strength of 10JNEX900 [24].

Destroyed samples during tests are shown in Fig. 14. It can be seen that the 10JNEX900 sample is highly deformed, which is consistent with the tested results shown in Fig. 13. The samples are broken after the strain is higher than 14 %. This means 10JNEX900 is able to withstand small defects. In other words, small defects only slightly reduce the mechanical strength of 10JNEX900. Since the mechanical strength of 10JNEX900 is stable and high, the degradation problem the 2605SA1 cores facing with can be avoided when 10JNEX900 is used.

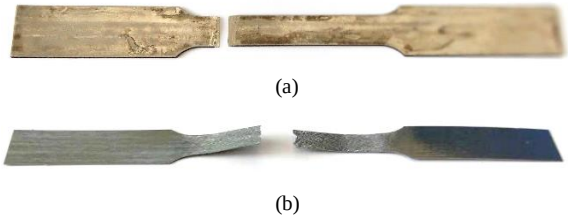

(a)

(b)

Fig. 14. Broken samples during mechanical strength tests. (a) 20-layer 2605SA1. (b) 10JNEX900.

III. Feasibility Study

To evaluate the feasibility of employing high-silicon steel 10JNEX900 for the proposed IPM rotor, the performances of the rotor made from 10JNEX900 in terms of mechanical, electromagnetic and thermal behaviors are evaluated. A prototype made from 2605SA1 is used as a benchmark. In this paper, the rotor made from 10JNEX900 core is named as HR (high-silicon steel rotor) and the corresponding motor is named as HM (high-silicon steel motor), while the rotor made from 2605SA1 core is named as AR (amorphous metal rotor) and the corresponding motor is named as AM (amorphous metal motor).

A. Rotor structure and specifications

In [22] an IPM rotor made from high mechanical strength and low core losses material is proposed. The feasibility of using 2605SA1 for the proposed rotor to improve the performance of the motors, such as higher power density and higher efficiency, is studied and confirmed. The structure of the IPM rotor and the parameters of a demonstrator motor are presented in Fig. 15 and Table II, respectively.

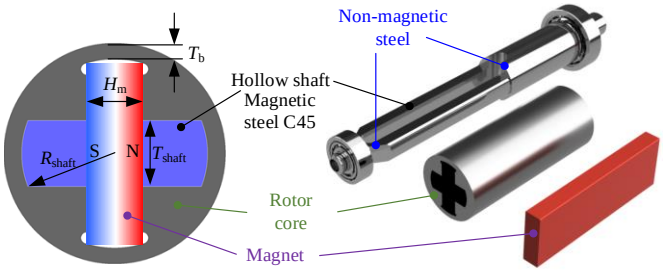

Fig. 15. Proposed IPM rotor for high-speed application [22].

TABLE II
Parameters of the Designed Demonstrator Motor

Parameter	Value
Maximum speed n_{max} (rpm)	125,000
Rated torque T_N (Nm)	1.2
Rotor diameter D_R (mm)	20
Air-gap length δ (mm)	0.5
Axial length L_{fe} (mm)	50
Flux bridge T_b (mm)	1.5
PM thickness H_m (mm)	5
Radius of shaft R_{shaft} (mm)	8.35
Shaft thickness T_{shaft} (mm)	6
Stator outer diameter D_S (mm)	64
Housing diameter D_h (mm)	84
Total length L_{total} (mm)	160

B. Mechanical stress analysis

To ensure that the rotors are safe at the maximum speed, the rotors' stresses are firstly analyzed. By using software Abaqus, the stresses at the maximum speed of the two rotors made from different core materials are simulated and compared in Fig. 16. It is clear that the maximum stresses locate at the flux bridges' inner contours of the rotor cores. Because of higher mass density of 10JNEX900, the maximum stress of HR is slightly higher than that of AR. The maximum stress of HR is 359 MPa, which is much lower than the tested yield strength (570 MPa) of the rotor core material. Since the mechanical strength of 10JNEX900 is stable, this safety margin is sufficient to run the HR to the maximum speed. The maximum stress of AR is 344 MPa. It is also much lower than the yield strength provided by the material manufacturer (700 MPa). However, based on the tested results of the 20-layer 2605SA1 samples, it is known that because the mechanical strength of 2605SA1 cores might be significantly reduced due to the influence of cutting, the 2605SA1 rotor core might be in risk of being destroyed. To solve this problem, as aforementioned, it is necessary to remove the defected layers or to adjust the cutting parameters of the machine to reduce the number of defected layers. Otherwise, a bigger flux bridge is needed so as to decrease the stress and to ensure that the rotor can reach the maximum speed. In this case, the torque and power densities will be correspondingly decreased. As this paper is not focused on solving the degradation problems of 2605SA1 rotor and the goal of the paper is to study whether 10JNEX900 is feasible for the proposed high-speed IPM rotor, the problems of 2605SA1 rotor are not further discussed.

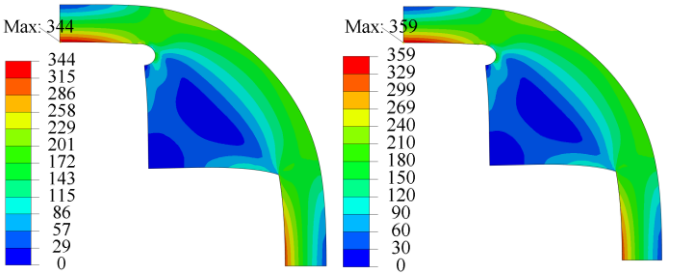

Fig. 16. Simulated mechanical stresses (Unit: MPa) in the rotor cores of different materials at 125,000 rpm. (a) 2605SA1. (b) 10JNEX900.

C. Electromagnetic performance

The electromagnetic performances of the two motors are predicted with the assistance of a finite element analysis (FEA) software Flux 2D. The no-load magnetic flux density distributions of the two motors are compared in Fig. 17. It clearly shows that the magnetic flux density at the flux bridge regions of HR is slightly higher than that of AR. This is because the saturation flux density of 10JNEX900 is higher than that of 2605SA1. Furthermore, the magnetic flux density of the shaft of HR is much lower than that of AR.

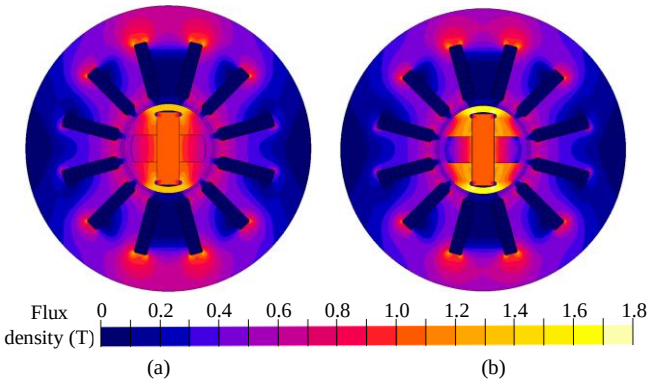

Fig. 17. Simulated no-load magnetic flux density distributions of the motors with different rotors. (a) 2605SA1. (b) 10JNEX900.

Because the flux leakage of HR is higher than that of AR, the air-gap PM excitation magnetic flux density of the former is lower than that of the latter as can be seen in Fig. 18.

When the amplitude of phase current is 50 A, the torque of the two motors is around 1.2 Nm. In this case, the magnetic flux density distributions of the two motors are compared in Fig. 19. The air-gap magnetic flux densities are compared in Fig. 20. It is found that HM has higher maximum flux density. Hence, it is believed that the HM has better overload ability.

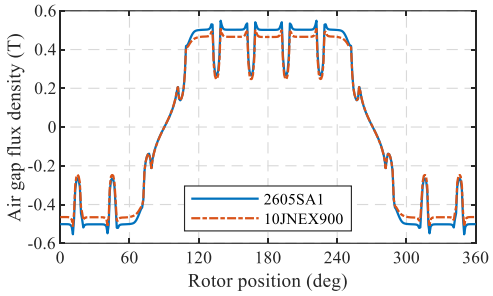

Fig. 18. Simulated no-load air-gap magnetic flux density radial field component of the two motors.

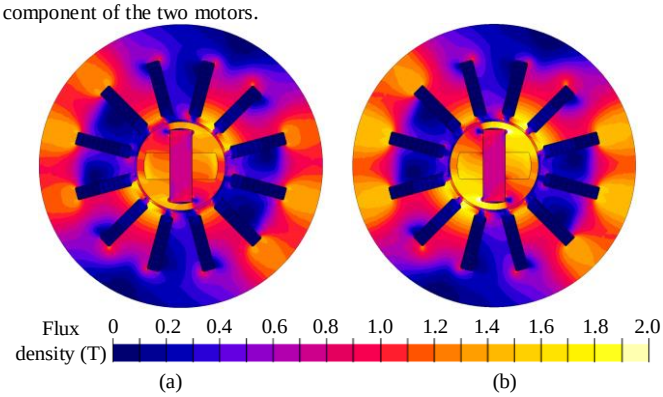

Fig. 19. Simulated magnetic flux density distributions of the motors with different rotors when the amplitude of phase current is 50 A. (a) 2605SA1. (b) 10JNEX900.

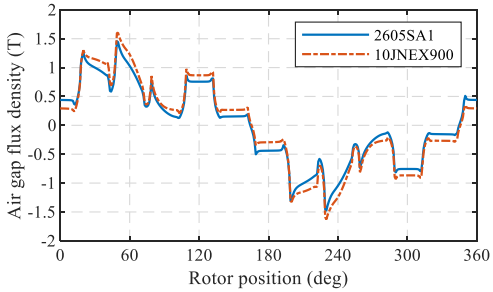

Fig. 20. Simulated air-gap magnetic flux density radial field component of the two motors when the amplitude of phase current is 50 A.

Because IPM motor not only generates magnetic torque, but also provides reluctance torque, it is necessary to use flux-weakening control to maximize the torque. When the phase RMS currents are 20 A and 40 A, respectively, the torque as a function of current leading angle of the two motors are compared in Fig. 21.

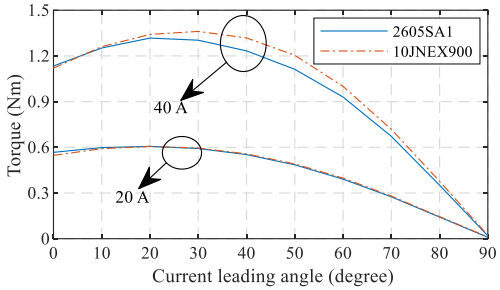

Fig. 21. Simulated torque as a function of current leading angle of the two motors.

It can be found that when the current leading angle is about 30 degrees, the torque of the two motors is maximized. Moreover, when the phase current is increased, the difference of the maximum torque of the two motors is increased. This is mainly because 10JNEX900 has higher saturation flux density than 2605SA1.

D. Losses and temperature rise prediction

Because high frequency occurs at high speeds, it is necessary to consider the influence of high-order current harmonics generated by PWM converters on the losses of the motors, including copper AC losses, rotor eddy current loss and so on. To better predict the losses of high-speed PM motors, coupled simulation between Matlab/Simulink and Flux 2D is applied. The structure of coupled simulation model is shown in Fig. 22. The control strategy is performed in Simulink, while the electromagnetic calculation is performed in Flux. The Simulink software receives necessary data such as phase currents, rotor position and torque from Flux, then proper space vector pulse width modulation (SVPWM) signals are calculated and sent to Flux. The electromagnetic performance of the motor will be calculated in Flux.

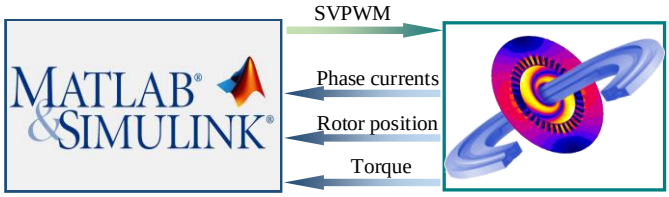

Fig. 22. Structure of coupled simulation to predict the electromagnetic performance of the high-speed PM motors.

In the coupled simulation, the eddy current losses in the PMs and copper windings are considered and they are calculated during simulation. Because the core losses are post-processed in Flux, they are not taken into consideration in the coupled simulation. To consider the copper AC losses in FEA simulation, individual conductors in the slots are modeled and they are set as solid conductor regions. Then all the conductors of one phase are connected in series in the electric circuit. The magnet and the shaft are also set as solid conductor regions to calculate their eddy current losses. These simulation methods are commonly employed and more details can be found in [31] to [33]. The core losses are calculated based on Bertotti equation and the variable coefficients of the iron loss equation are extracted from the above measured loss data [34]. The rotor air-friction losses are calculated by using the introduced method in [22].

At maximum speed and rated torque, the losses of the two motors are compared in Table III. Because HR can generate higher torque, the phase current needed to generate the rated torque is lower and this results in lower winding losses. Due to higher core losses of 10JNEX900 than those of 2605SA1, the HR has higher core losses than the AR. The shaft loss of HR is lower than that of the AR, this is because the saturation flux density of 10JNEX900 is higher than that of 2605SA1 and less flux lines pass though the shaft of the HR. Because the stator core losses of the HM are higher than the AM, the total losses of the two motors are comparable.

TABLE III
MOTOR CURRENTS AND LOSSES AT 125,000 RPM AND 1.2 NM WHEN THE PWM FREQUENCY IS 50 KHZ AND THE DC-BUS VOLTAGE IS 600 V

Rotor core material	2605SA1	10JNEX900
Phase RMS current (A)	42.39	37.88
Current leading angle (deg)	40	30
Shaft loss (W)	41.31	31.14
PM loss (W)	26.00	24.04
Rotor core losses (W)	5.08	9.60
Stator core losses (W)	318.06	383.55
Stator winding losses (W)	436.08	393.48
Rotor air-friction losses (W)	15.96	15.96
Total losses (W)	842.49	857.77
Efficiency	94.91 %	94.82 %

Due to high-speed operation, the power of the two motors is very high. The difference in efficiency between them is very small. The criterion to evaluate the two motors is the temperature rise. In this paper, water-cooled method is used. Hence, a computational fluid dynamic (CFD) software Star CCM+ is applied. To consider the temperature difference of the windings at different positions, precise three dimensional model is built and the mesh of the model are presented in Fig. 23. To improve the cooling performance, the stator is encapsulated with high thermal conductivity epoxy resin.

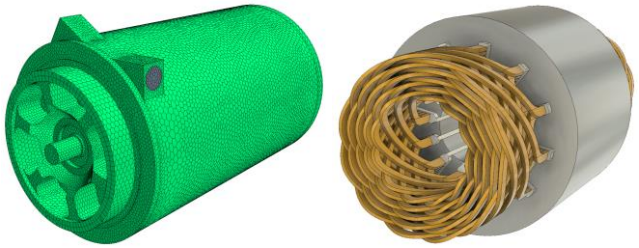

Fig. 23. Mesh of the CFD model with precise 3-D stator structure.

In the simulation models, the ambient and the inlet water temperatures are 300 K (26.85 °C). The inlet water velocity is 1 m/s. The temperature distributions of the two motors at maximum speed and rated torque are compared in Fig. 24. Because the losses of copper windings close to the air gap are higher than those at the bottom of slots and the cooling

condition at the bottom is better, the windings close to the air gap is much hotter than the bottom windings. The maximum temperatures of each component of the two motors are listed and compared in Table IV. It is found that the HM has lower temperature than the AM.

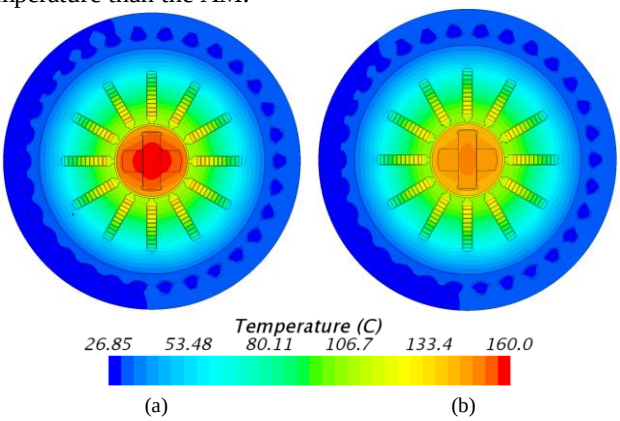

Fig. 24. Simulated temperature distributions on radial cross section of the motors made from different rotor core materials. (a) 2605SA1. (b) 10JNEX900.

TABLE IV
MAXIMUM TEMPERATURE OF THE TWO MOTORS AT 125,000 RPM AND 1.2 NM

Rotor core material	2605SA1	10JNEX900
Stator (°C)	138.2	132.9
Rotor (°C)	159.5	149.3

IV. VERIFICATION BY TESTING OF A PROTOTYPE

To verify the FEA and CFD analysis results, the tested results of a prototype made from 2605SA1 are compared with the simulated results. The manufacturing processes of the proposed IPM rotor made from 2605SA1 are illustrated in Fig. 25. 2605SA1 ribbons are firstly stacked and solidified and then are cut by wire electrical discharge machining method. When 10JNEX900 is used, the same methods can be used. Alternatively, 10JNEX900 core can be cut by laser. The hollow shaft is firstly welded by friction and then is slotted. The manufactured rotor is about 200 g while the whole motor is about 2.8 kg in weight.

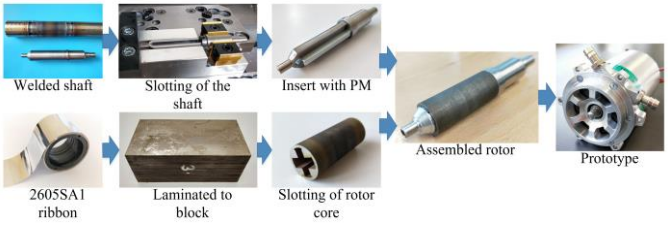

Fig. 25. Manufacturing processes of the proposed IPM rotor made from 2605SA1.

The test bench of the designed high-speed IPM motors is shown in Fig. 26. Two prototypes are directly connected through a coupling. A strain gage based torque sensor TS70 produced by ME-Meßsystem GmbH is connected at the end-cap of the tested prototype. During the test, one of the prototypes is driven as a motor, while the other is driven as a generator.

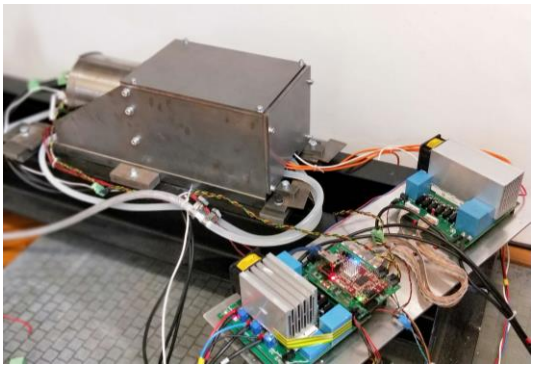

Fig. 26. Picture of the test bench.

The no-load back-EMF is firstly tested and it is compared with FEA result as presented in Fig. 27. The FEA results agree well with the experimental results. The error between FEA and test at 60,000 rpm is about 6.3 %. In views of engineering, this error is acceptable. The FEA analysis is correct and credible. Due to lower air-gap flux density of HM at no-load condition as shown in Fig. 18, the back-EMF of HM is slightly lower than that of AM.

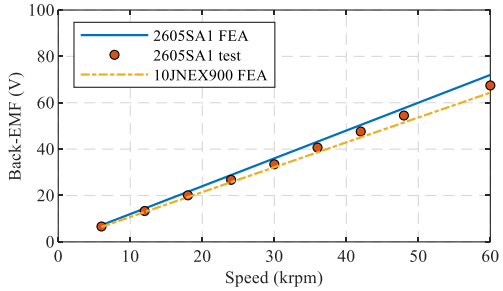

Fig. 27. Comparison of simulated and tested no-load back EMF as a function of speed.

The torque as a function of current amplitude is presented in Fig. 28. It is found that HM has slightly higher torque than AM. Since the tested back-EMF of AM is a little lower than the FEA results, the tested torque is also a little lower. The decrease of the experimental back-EMF and torque compared to the FEA results might be mainly caused by the flux leakage at the ends of the shaft, the deviation of the stacking factor and the deviation of electromagnetic properties of 2605SA1 rotor core.

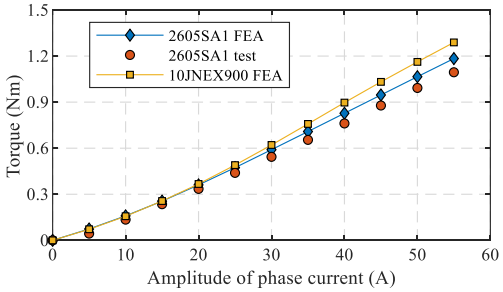

Fig. 28. Comparison of simulated and tested torque as a function of phase current.

The thermal behavior of the prototype is also tested. The temperature rises of the prototype at 10,000 rpm, 0.83 Nm and 30,000 rpm, 0.51 Nm are measured and compared with the CFD calculation results as listed in Table V. Since the influence of PWM converter on the losses of the motor is considered through coupled simulation, the errors between CFD and experimental results are quite small. Hence, the

analysis methods used in this paper are feasible and convincing, and the analysis results of the motors with different rotor core materials are credible.

TABLE V
TEMPERATURE RISES COMPARISON OF THE PROTOTYPE AT LOAD CONDITIONS

Speed and load	Phase RMS current (A)	Temperature rise (K)	CFD	Experimental
10,000 rpm, 0.83 Nm	31.62	Windings	28.8	31.0
		Rotor	40.2	36.1
30,000 rpm, 0.51 Nm	21.21	Windings	17.6	17.1
		Rotor	42.6	37.4

Note: the maximum temperature rise at the windings is located at the end-winding.

V. CONCLUSION

Amorphous metal 2605SA1 is beneficial in improving the performance of high-speed interior permanent-magnet (IPM) rotors. However, the mechanical strength of this material is easily degraded during mechanical processes, which may cause failures of the rotors and results in low yield ratio of massive production. Hence, high-silicon steel 10JNEX900 is considered in this paper as an alternative to 2605SA1. To evaluate the feasibility of employing 10JNEX900 for the proposed high-speed IPM rotor, the electromagnetic and mechanical properties of 10JNEX900 are tested and compared with 2605SA1. The experimental results of the materials show that the mechanical strength of 10JNEX900 is stable, around 570 MPa. Then, by using the tested data, the performance of the designed motors made from the above mentioned materials in terms of electromagnetic, mechanical and thermal aspects is predicted. The motor made from 2605SA1 is used as a benchmark for comparison. The analysis results show that the motor made from 10JNEX900 has similar performance to the motor made from 2605SA1. By testing of a prototype made from 2605SA1, the accuracy of simulation results is assessed and confirmed. It is believed that the analysis methods in the paper for the proposed motors are credible. Based on our study, it is feasible to use 10JNEX900 in our proposed IPM motor and this material has high potential for massive production of the proposed IPM motor.

VI. REFERENCES

[1] D. Gerada, A. Mebarki, N. L. Brown, C. Gerada, A. Cavagnino and A. Boglietti, "High-speed electrical machines: technologies, trends, and developments," *IEEE Trans. Ind. Electron.*, vol. 61, no. 6, pp. 2946-2959, June 2014.

[2] T. Noguchi, Y. Takata, Y. Yamashita and S. Ibaraki, "160,000-r/min, 2.7-kW electric drive of supercharger for automobiles," 2005 *Int. Conf. on Power Electron. and Drives Systems*, Kuala Lumpur, 2005, pp. 1380-1385.

[3] D. Krahenbuhl, C. Zwyssig, H. Weser and J. W. Kolar, "A miniature 500 000-r/min electrically driven turbocompressor," *IEEE Trans. Ind. Appl.*, vol. 46, no. 6, pp. 2459-2466, Nov.-Dec. 2010.

[4] S. M. Jang, H. W. Cho and S. K. Choi, "Design and analysis of a high-speed brushless DC motor for centrifugal compressor," *IEEE Trans. Magn.*, vol. 43, no. 6, pp. 2573-2575, June 2007.

[5] M. S. Lim, J. M. Kim, Y. S. Hwang and J. P. Hong, "Design of an ultra-high-speed permanent-magnet motor for an electric turbocharger considering speed response characteristics," *IEEE/ASME Trans. Mechatronics*, vol. 22, no. 2, pp. 774-784, April 2017.

[6] C. Zwyssig, J. W. Kolar, W. Thaler and M. Vohrer, "Design of a 100 W, 500000 rpm permanent-magnet generator for mesoscale gas turbines," *Fourtieth IAS Annual Meeting. Conf. Record of the 2005 Ind. Appl. Conf.*, 2005., 2005, pp. 253-260 Vol. 1.

[7] C. Zwyssig, M. Duerr, D. Hassler and J. W. Kolar, "An ultra-high-speed, 500000 rpm, 1 kW electrical drive system," *Power Convers. Conf. - Nagoya*, Nagoya, 2007, pp. 1577-1583.

[8] P. D. Pfister and Y. Perriard, "Very-high-speed slotless permanent-magnet motors: Analytical Modeling, Optimization, Design, and Torque Measurement Methods," *IEEE Trans. Ind. Electron.*, vol. 57, no. 1, pp. 296-303, Jan. 2010.

[9] A. Tüysüz, M. Steichen, C. Zwyssig and J. W. Kolar, "Advanced cooling concepts for ultra-high-speed machines," *9th Int. Conf. on Power Electron. and ECCE Asia (ICPE-ECCE Asia)*, Seoul, 2015, pp. 2194-2202.

[10] C. Zwyssig, S. D. Round and J. W. Kolar, "An ultra-high-speed, low power electrical drive system," *IEEE Trans. Ind. Electron.*, vol. 55, no. 2, pp. 577-585, Feb. 2008.

[11] D. K. Hong, B. C. Woo, J. Y. Lee and D. H. Koo, "Ultra high speed motor supported by air foil bearings for air blower cooling fuel cells," *IEEE Trans. Magn.*, vol. 48, no. 2, pp. 871-874, Feb. 2012.

[12] T. Abe, T. Higuchi, K. Shigematsu and J. Oyama, "The system simulation for small size and ultra-high speed motor drive system using coupled analysis," *European Conf. on Power Electron. and Appl.*, Aalborg, 2007, pp. 1-8.

[13] J. H. Ahn, J. Y. Choi, C. H. Park, C. Han, C. W. Kim and T. G. Yoon, "Correlation between rotor vibration and mechanical stress in ultra-high-speed permanent magnet synchronous motors," *IEEE Trans. Magn.*, vol. 53, no. 11, pp. 1-6, Nov. 2017.

[14] T. Noguchi, Y. Takata, Y. Yamashita, Y. Komatsu, and S. Ibaraki, "220,000-r/min, 2-kW PM motor drive for turbocharger," *Electrical Engineering in Japan*, Vol. 161, No. 3, pp. 854-861, 2007.

[15] T. Schneider and A. Binder, "Design and evaluation of a 60 000 rpm permanent magnet bearingless high speed motor," *7th Int. Conf. on Power Electron. and Drive Systems*, Bangkok, 2007, pp. 1-8.

[16] T. Noguchi and T. Wada, "1.5-kW, 150,000-r/min ultra high-speed PM motor fed by 12-V power supply for automotive supercharger," *European Conf. on Power Electron. and Appl.*, Barcelona, 2009, pp. 1-10.

[17] A. Binder, T. Schneider and M. Klohr, "Fixation of buried and surface-mounted magnets in high-speed permanent-magnet synchronous machines," *IEEE Trans. Ind. Appl.*, vol. 42, no. 4, pp. 1031-1037, July-Aug. 2006.

[18] H. Cho, S. Jang and S. Choi, "A design approach to reduce rotor losses in high-speed permanent magnet machine for turbo-compressor," *IEEE Trans. Magn.*, vol. 42, no. 10, pp. 3521-3523, Oct. 2006.

[19] W. Li, H. Qiu, X. Zhang, J. Cao, S. Zhang and R. Yi, "Influence of rotor-sleeve electromagnetic characteristics on high-speed permanent-magnet generator," *IEEE Trans. Ind. Electron.*, vol. 61, no. 6, pp. 3030-3037, June 2014.

[20] S. Kim, Y. Kim, G. Lee and J. Hong, "A Novel rotor configuration and experimental verification of interior PM synchronous motor for high-speed applications," *IEEE Trans. Magn.*, vol. 48, no. 2, pp. 843-846, Feb. 2012.

[21] J. Zhang, *et al.*, "Evaluation of applying retaining shield rotor for high-speed interior permanent magnet motors," *IEEE Trans. Magn.*, vol. 51, no. 3, pp. 1-4, March 2015.

[22] Y. Liu, J. Ou, M. Schiefer, P. Breining, F. Grilli and M. Doppelbauer, "Application of an amorphous core to an ultra-high-speed sleeve-free interior permanent-magnet rotor," *IEEE Trans. Ind. Electron.*, vol. 65, no. 11, pp. 8498-8509, Nov. 2018.

[23] K. Shoji, N. Misao, and H. Tatsuhiko, "Recent progress of high silicon electrical steel in JFE steel," *JFE Technical Report*, no. 21, pp. 14-19, Mar. 2016.

[24] J. Ou, Y. Liu, P. Breining, T. Gietzelt, T. Wunsch and M. Doppelbauer, "Study of the electromagnetic and mechanical properties of a high-silicon steel for a high-speed interior PM rotor," *22nd International Conference on Electrical Machines and Systems (ICEMS)*, Harbin, China, 2019, pp. 1-4.

[25] [online] Available: https://metglas.com/wp-content/uploads/2016/12/Amorphous-Alloys-for-Transformer-Cores-.pdf.

[26] [online] Available: https://www.jfe-steel.co.jp/en/products/electrical/catalog/f2e-001.pdf.

[27] Z. Wang, Y. Enomoto, R. Masaki, K. Souma, H. Itabashi and S. Tanigawa, "Development of a high speed motor using amorphous metal cores," in *8th International Conference on Power Electronics - ECCE Asia*, Jeju, 2011, pp. 1940-1945.
[28] Y.R. Wang, "Modelling and characterisation of losses in nanocrystalline cores," Ph.D. dissertation, Faculty of Engineering and Physical Sciences, University of Manchester, Manchester, UK, 2015.
[29] M. Veigel, P. Winzer, J. Richter and M. Doppel-bauer, "New FPGA-based and inline-capable measuring method for the identification of magnetic losses in electrical steel," *5th Int. Electric Drives Production Conf. (EDPC)*, pp. 1-6. Nuremberg, 2015.
[30] J. Ou, Y. Liu, P. Breining, M. Schiefer and M. Doppelbauer, "Experimental study of the amorphous magnetic material for high-speed sleeve-free PM rotor application," *IEEE Trans. Ind. Electron.*, vol. 67, no. 6, pp. 4422-4432, June 2020.
[31] M. Schenk and R. W. De Doncker, "Automated copper loss calculation for switched reluctance machines," *2013 15th European Conference on Power Electronics and Applications (EPE)*, Lille, 2013, pp. 1-9.
[32] M. Popescu and D. G. Dorrell, "Proximity losses in the windings of high speed brushless permanent magnet AC motors with single tooth windings and parallel paths," *IEEE Trans. Magn.*, vol. 49, no. 7, pp. 3913-3916, July 2013.
[33] J. Ou, Y. Liu, D. Liang and M. Doppelbauer, "Investigation of PM eddy current losses in surface-mounted PM motors caused by PWM," *IEEE Trans. Power Electron.*, vol. 34, no. 11, pp. 11253-11263, Nov. 2019.
[34] M. M. J. Al-Ani, J. Carter and M. L. Jupp, "Comparison of electromagnetic performance and power losses of a high-speed machine fed by PWM and PAM inverter strategies," *8th IET International Conference on Power Electronics, Machines and Drives (PEMD 2016)*, Glasgow, 2016